


 Cite this: *RSC Adv.*, 2024, 14, 7276

# Explainable machine-learning predictions for catalysts in CO<sub>2</sub>-assisted propane oxidative dehydrogenation†

 Hongyu Liu,  ‡<sup>ab</sup> Kangyu Liu,  ‡<sup>b</sup> Hairuo Zhu,  <sup>a</sup> Weiqing Guo<sup>a</sup> and Yuming Li<sup>\*a</sup>

Propylene is an important raw material in the chemical industry that needs new routes for its production to meet the demand. The CO<sub>2</sub>-assisted oxidative dehydrogenation of propane (CO<sub>2</sub>-ODHP) represents an ideal way to produce propylene and uses the greenhouse gas CO<sub>2</sub>. The design of catalysts with high efficiency is crucial in CO<sub>2</sub>-ODHP research. Data-driven machine learning is currently of great interest and gaining popularity in the heterogeneous catalysis field for guiding catalyst development. In this study, the reaction results of CO<sub>2</sub>-ODHP reported in the literature are combined and analyzed with varied machine learning algorithms such as artificial neural network (ANN), *k*-nearest neighbors (KNN), support vector regression (SVR) and random forest regression (RF) and were used to predict the propylene space-time yield. Specifically, the RF method serves as a superior performing algorithm for propane conversion and propylene selectivity prediction, and SHapley Additive exPlanations (SHAP) based on the Shapley value performs fine model interpretation. Reaction conditions and chemical components show different impacts on catalytic performance. The work provides a valuable perspective for the machine learning in light alkane conversion, and helps us to design catalyst by catalytic performance hidden in the data of literatures.

 Received 16th January 2024  
Accepted 17th February 2024

DOI: 10.1039/d4ra00406j

[rsc.li/rsc-advances](https://rsc.li/rsc-advances)

## 1 Introduction

Propylene is an important raw material in the production of various petrochemicals, including polypropylene and rubber.<sup>1</sup> At present, propylene is mainly produced *via* steam cracking and fluid catalytic cracking. With the increasing demand for propylene in the global industrial market, new propylene production routes, especially environment-friendly and energy-efficient ones, are urgently needed.<sup>2</sup> With recent development in shale gas exploitation techniques, abundant light alkanes can be produced, which thus gives a great chance for the application of propane dehydrogenation.<sup>3</sup> Compared with propane nonoxidative dehydrogenation, propane oxidative dehydrogenation shows good stability owing to the existence of oxidants (*e.g.* O<sub>2</sub>, N<sub>2</sub>O, CO<sub>2</sub>, SO<sub>2</sub> and Cl<sub>2</sub>).<sup>1,2</sup> Specifically, the CO<sub>2</sub>-assisted oxidative dehydrogenation of propane (CO<sub>2</sub>-ODHP) is one of the most prominent routes for its advantage in the cooperative conversion of CO<sub>2</sub> and propane.<sup>4,5</sup>

CO<sub>2</sub>-ODHP uses CO<sub>2</sub> as a mild oxidant to transform propane into propylene. During this catalytic process (as shown in Table 1), CO<sub>2</sub> is directly converted to CO, which exhibits a great application in the syngas reaction (CO<sub>2</sub> + C<sub>3</sub>H<sub>8</sub> → CO + C<sub>3</sub>H<sub>6</sub> + H<sub>2</sub>O).<sup>6</sup> Compared with propane nonoxidative dehydrogenation (C<sub>3</sub>H<sub>8</sub> → C<sub>3</sub>H<sub>6</sub> + H<sub>2</sub>), CO<sub>2</sub>-ODHP can improve the equilibrium of propane conversion *via* propane dry reforming during the reaction (3CO<sub>2</sub> + C<sub>3</sub>H<sub>8</sub> → 6CO + 4H<sub>2</sub>). Besides, the presence of CO<sub>2</sub> facilitates the removal of the deposited coke *via* the Boudouard reaction (C + CO<sub>2</sub> → 2CO), which stabilizes the CO<sub>2</sub>-ODHP reaction.

There are two reaction mechanisms involved in CO<sub>2</sub>-ODHP, namely the Mars–van-Krevelen mechanism and a coupling mechanism between the reverse water gas shift reaction and the propane dehydrogenation reaction.<sup>2</sup> The Mars–van-Krevelen mechanism is also called the lattice oxygen mechanism. It usually occurs on transition metal oxide-based catalysts. Propane is first oxidized to propylene by lattice oxygen on a metal oxide catalyst, and an oxygen vacancy is formed on the metal oxide. At this time, CO<sub>2</sub> provides an oxygen atom to supplement the lattice oxygen vacancy on the catalyst so that the whole reaction is balanced. The lattice oxygen on the catalyst is directly involved in the reaction. The coupling mechanism holds that under appropriate reaction conditions, the reverse water gas shift reaction (RWGS) will be coupled with the propane dehydrogenation reaction, and jointly promote the process.

<sup>a</sup>State Key Laboratory of Heavy Oil Processing, China University of Petroleum, Beijing, 102249, PR China. E-mail: liyuming@cup.edu.cn

<sup>b</sup>National Engineering Research Center for Petroleum Refining Technology and Catalyst, Research Institute of Petroleum Progressing Co., Ltd., SINOPEC, Beijing 100083, China

† Electronic supplementary information (ESI) available. See DOI: <https://doi.org/10.1039/d4ra00406j>

‡ These authors contributed equally.



Table 1 The thermodynamic parameters of reactions in CO<sub>2</sub>-ODHP

	CO <sub>2</sub> -ODHP reaction steps	$\Delta H_{25\text{ }^\circ\text{C}}$ (kJ mol <sup>-1</sup> )	$\Delta G_{25\text{ }^\circ\text{C}}$ (kJ mol <sup>-1</sup> )
1	$\text{C}_3\text{H}_8 \rightleftharpoons \text{C}_3\text{H}_6 + \text{H}_2$	+124	+86
2	$\text{C}_3\text{H}_8 + \text{CO}_2 \rightleftharpoons \text{C}_3\text{H}_6 + \text{CO} + \text{H}_2\text{O}$	+164	+115
3	$\text{CO}_2 + \text{H}_2 \rightleftharpoons \text{CO} + \text{H}_2\text{O}$	+41	+29
4	$\text{CO}_2 + \text{C} \rightleftharpoons 2\text{CO}$	+172	+120
5	$\text{C}_3\text{H}_8 + 3\text{CO}_2 \rightleftharpoons 6\text{CO} + 4\text{H}_2$	+621	+383
6	$\text{C}_3\text{H}_8 \rightleftharpoons \text{C}_2\text{H}_4 + \text{CH}_4$	+82	+41
7	$\text{C}_3\text{H}_8 \rightleftharpoons \text{CH}_4 + 2\text{C} + 2\text{H}_2$	+29	-27
8	$\text{C}_3\text{H}_8 \rightleftharpoons 3\text{C} + 4\text{H}_2$	+104	-23

Previous CO<sub>2</sub>-ODHP studies were mainly focused on Cr-,<sup>7,8</sup> V-,<sup>9,10</sup> Ga-,<sup>11,12</sup> and In-<sup>13,14</sup> based catalysts. Bu *et al.* prepared a copper-modified Ga-MFI zeolite (Cu/Ga-MFI) and introduced it into CO<sub>2</sub>-ODHP.<sup>15</sup> It was reported that the Ga atoms in the MFI framework can give a moderate acid strength, and the Cu species can provide an appropriate Brønsted/Lewis acid distribution, which will enhance the catalytic performance. Thus, the aromatics selectivity of 73% at propane conversion of 93.6% was achieved. A series of M@ZSM-5 (M = V-, Ga-, Ti-, or Ni-oxide) combined with CaO catalysts was prepared by Lawson *et al.*<sup>16</sup> The catalytic performance of these catalysts in CO<sub>2</sub>-ODHP revealed that the Ti-doped catalyst generated the best balance of CO<sub>2</sub> conversion (76%) and propylene selectivity (39%), due to the high dispersion of TiO<sub>2</sub>. The variation of the metal dopant could control the catalytic performance. Mo<sub>2</sub>C, as a novel catalyst, was found to be active in CO<sub>2</sub>-ODHP by Sullivan *et al.*<sup>17</sup> The kinetic models were carefully investigated, and the two-site dehydrogenation mechanism can provide proper explanation for the good reaction results of Mo<sub>2</sub>C. Nevertheless, the current development of catalysts in CO<sub>2</sub>-ODHP is mainly based on trial-and-error experiments. For the design of new catalysts in high activity, it is important to predict catalytic performance and the influencing factors.

Support modulation, additive modification, and preparation-method variations are efficient methods for enhancing the catalytic performance.<sup>5</sup> During the past decades, large amounts of experimental data have been reported in the propane conversion field. However, varied methods of the reaction conditions during CO<sub>2</sub>-ODHP reaction in the reported literature have made it complex to decouple the modulation mechanism, which thus brings a great challenge to revealing the fine correlation between the catalyst composition and their catalytic performance.<sup>18,19</sup> Thus, establishing an efficient and accurate relationship between the catalyst composition and CO<sub>2</sub>-ODHP performance would provide reliable guidance for catalyst design and developing effective catalyst systems.

Recently, owing to the fast development of computer science, especially machine learning, sophisticated and complex nonlinear models (*e.g.* artificial neural networks, kernel regression, random forest, *etc.*) have achieved a great application in the heterogeneous catalysis fields.<sup>20</sup> Notably, prediction of the impact of input process variables on the catalysis processes is the key to enhancing the catalytic performance.

Based on machine learning with the combination of vast data in the references, relative empirical models can be trained based on these data.<sup>21</sup> Hereafter, these models can offer advice on catalyst design, predict the impact of relative parameters on the catalytic activity,<sup>22-24</sup> explain the structure-activity relationship<sup>25</sup> and evaluate kinetic data.<sup>26</sup> For the catalyst design, Guo *et al.*<sup>27</sup> analyzed and predicted the organic additives during Cu-catalyzed CO<sub>2</sub> reduction with the XGBoost algorithm and found that aliphatic hydroxyl-containing additives can improve the formation of Cu<sub>2</sub>O in the cubic phase, which is crucial for the catalytic performance. Especially with the combination of DFT calculations, catalysts with excellent catalytic performance can be screened out.<sup>28-30</sup> Liu's group successfully predicted the transition energy variation of reactant molecules during F-T synthesis and ethylene oxidation with the assistance of DFT and machine learning, which can guide the catalyst design.<sup>31,32</sup> Moreover, due to the large number of literature reports, it is difficult to establish a structure-activity relationship for purposeful catalyst preparation or to identify suitable experimental conditions. Yang *et al.*<sup>33</sup> used decision tree analysis to elucidate the influence of catalyst compositions, promoters, supports, precursors, preparation methods, reaction conditions, *etc.*, on the catalytic performance of CO<sub>2</sub> hydrogenation. The selectivity-determining descriptors can be revealed, and their findings in the catalyst design were also proved by experiments. Similar applications of machine learning on oxygen evolution reaction and chemical looping oxidative dehydrogenation of propane are also reported.<sup>34,35</sup>

To the best of our knowledge, the application of machine learning in CO<sub>2</sub>-ODHP for catalysis analysis has still not been reported. In the present work, the statistical correlations between catalyst composition, reaction parameters, and catalytic performance of CO<sub>2</sub>-ODHP reaction from previous literature studies are established based on a series of mathematical models, which were constructed using the artificial neural network (ANN), support vector regressor (SVR), random forest regressor (RF) and *k*-nearest neighbor (KNN) algorithms. In addition, we also applied the SHapley Additive exPlanations (SHAP) methodology on the collected dataset to identify the input variables with a great impact on the catalyst performance and revealed the effect of the important variables on the space-time yield of propylene, propane conversion and propylene selectivity in CO<sub>2</sub>-ODHP.



## 2 Data and methods

### 2.1 Catalytic reaction dataset of CO<sub>2</sub>-ODHP

In this study, CO<sub>2</sub>-ODHP reaction results reported in the literature were collected, and these data in the MS Excel format are loaded as the ESI.† We excluded mainly the reaction conditions including temperature, CO<sub>2</sub> concentration, C<sub>3</sub>H<sub>8</sub> concentration, WHSV, *etc.*, catalyst components, and catalytic performance (space-time yield of propylene, propane conversion and propylene selectivity), which are all described in the dataset.

### 2.2 Machine learning

All the algorithms were run using the open-source code Scikit-learn package in the Python 3 environment.<sup>36</sup> The original 270 data were randomly divided into the training set and testing set to guarantee the accuracy of the models. Unsupervised learning algorithms were used to visualize the dataset. That is, *k*-means clustering algorithm<sup>37</sup> was first introduced to group similar samples together, and principle component analysis (PCA) and *t*-distributed stochastic neighbor embedding (*t*-SNE), which are widely used as the unsupervised machine learning tools for data analysis and data dimension reduction.<sup>38</sup> The Pearson correlation was used to measure a linear correlation between two variables. This can give information about the relationship between these variables using a linear or monotonic function.

Hereafter, four kinds of machine learning algorithms (ANN, SVR, RF and KNN) were used to obtain reliable qualitative and quantitative analysis results.<sup>39–43</sup> The brain's biological neural network consists of about 100 billion neurons, which are the basic processing units of the brain. These neurons perform their functions through huge connections between each other. ANN is inspired by its biological counterparts. It consists of an input layer and an output layer, where the input layer receives data from the dataset, and one or more hidden layers process the data. The output layer provides network-based functions for one or more data points. SVR is one of the most common applications of the support vector machines, which can be used for regression analysis. It finds a regression plane that makes all the data in a set closest to a regression plane. A margin of width  $\epsilon$  represents the accuracy, and the points within the  $2\epsilon$  interval are closest to the regression plane. It is considered that the prediction results of these points are more reliable. Thus, the aim of SVR is to contain maximum data within the margin. RF is an algorithm that integrates multiple trees through the idea of ensemble learning. Its basic unit is the decision tree, a branch of machine learning. Random forest is a classifier containing many decision trees, which can be used for both classification and regression problems. It is also known to work well even with very large datasets. Thus, RF is quite popular in the chemistry field, and the result is easy to interpret. KNN algorithm is a memory-based model, and it finds the *K* instances that are most adjacent to the new input instance in the training data set. If most of the *K* instances belong to a certain class, the input instance is classified into this class. KNN is mostly used for classification, and it is also suitable for regression analysis. The parameter *K* is important for the performance of KNN.

Two indexes, the root-mean-square error (RMSE) and the coefficient of determination value ( $R^2$  score) were introduced to analyze the prediction errors and evaluate the performance of different models, which were calculated using eqn (1) and (2). After selecting the RF algorithm as the best one, a grid search with 5-fold cross-validation was employed. Grid search is an exhaustive method that can find the optimal hyperparameters of the machine learning model. The key hyperparameters tested in this work are listed in the ESI in Table S1.† SHapley Additive exPlanations (SHAP) were used to interpret the model predictions.<sup>40</sup> In this work, tree SHAP, a variant of SHAP to provide explanations for the individual predictions made by RF was used.

$$\text{RMSE} = \sqrt{\frac{1}{n} \sum_{i=1}^n (y_i - \hat{y}_i)^2} \quad (1)$$

$$R^2 = 1 - \frac{\sum_{i=1}^n (y_i - \hat{y}_i)^2}{\sum_{i=1}^n (y_i - \bar{y}_i)^2} \quad (2)$$

where  $y_i$  means the predicted value by machine learning,  $\hat{y}_i$  denotes the real reaction result, and  $\bar{y}_i$  is the average value of the real reaction results.

## 3 Results and discussion

### 3.1 Data analysis

The conversion–selectivity relationship and reaction conditions analysis are shown in Fig. 1. Cr-, V-, Ga-, In-, Zn-, *etc.*, based catalysts are the main catalysts reported in the literature related to CO<sub>2</sub>-ODHP. The commonly used supports are SiO<sub>2</sub>, Al<sub>2</sub>O<sub>3</sub> and ZrO<sub>2</sub>-based oxides. To visualize the catalytic performance of all the catalysts, a propane conversion–propylene selectivity relationship is established and shown in Fig. 1a. It is quite evident that Cr- and V-based catalysts, the most extensively investigated ones, show higher propylene selectivity when propane

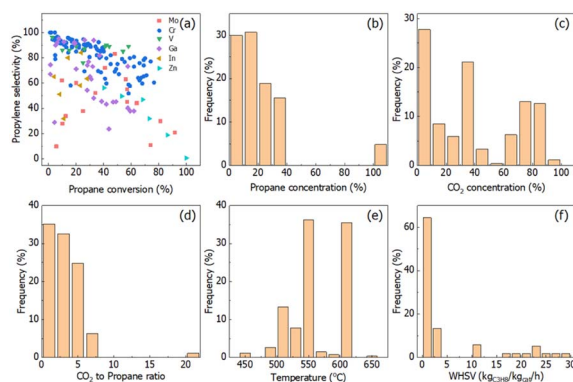


Fig. 1 (a) Propylene selectivity as a function of propane conversion for catalysts in the literature data labeled with specific colors. The examined conditions include (b) propane concentration, (c) CO<sub>2</sub> concentration, (d) CO<sub>2</sub> to propane molar ratio in the feed, (e) reaction temperature, and (f) weight hourly space velocity (WHSV).



conversion is lower than 50%, while the research for the catalytic performance at higher propane conversion (>80%) is still scarce. Moreover, Ga-based samples exhibit potential as a new kind of catalyst system with high selectivity at low propane conversion. It is clearly shown that the conversion–selectivity trade-off can be found for all the catalysts in the literature.

It is well known that the reaction conditions exert a large impact on the reaction results. For propane activation, propane concentration at a lower level is beneficial for propylene selectivity and propane conversion, and in more than half of the reported CO<sub>2</sub>-ODHP reactions <20% of propane concentration was chosen, as shown in Fig. 1b. For CO<sub>2</sub>, its concentration distribution has been chosen randomly (Fig. 1c), while, the ratio of CO<sub>2</sub> to propane concentration is always lower than 5 (Fig. 1d). Conventionally, the reaction temperature and weight hourly space velocity (WHSV) are crucial for both propane conversion and propylene selectivity. More than 70% of the reactions were carried on at the reaction temperature in the range of 550–600 °C, and WHSV of lower than 5 kg<sub>C<sub>3</sub>H<sub>8</sub></sub> kg<sub>cat</sub><sup>-1</sup> h<sup>-1</sup> was always used.

The Pearson correlation coefficient between the input variables and the targeted catalytic performance can reflect the degree of correlation between them. A higher Pearson correlation coefficient indicates a tighter positive correlation and *vice versa*. Reaction conditions are used as input variables, and catalytic performance, including the space-time yield of propylene (abbreviated as STY), propane conversion and propylene selectivity are the output variables. The color bar indicates correlation among descriptors, where deep color presents negative values and light color presents positive values. All the values of correlation are in the range of –1 to 1. It can be seen from Fig. 2 that, different reaction conditions are uncorrelated which can be determined by the Pearson correlation. For the correlation between the reaction conditions and catalytic performance, WHSV exhibits a relatively high positive correlation with an STY value (0.79), indicating that the increase of WHSV leads to a high STY value. For the Pearson correlation between the catalyst chemical composition and catalytic performance, no significant correlation could be observed (thus, the figure is not shown here).

To visualize in detail the relationship between the chemical composition and catalytic performance, twelve elements with higher average weight loading calculated from the reported literature were chosen and plotted with the STY values (Fig. S1†). The figures show that there is no obvious relationship

between chemical components and the STY value, which indicates that the influence of the chemical composition on catalytic performance cannot be directly established. Similar figures are drawn with reaction conditions and the STY value (Fig. S2†). It can be seen that higher STY values are skewed in the conditions with lower propane concentration, higher WHSV, and lower CO<sub>2</sub>-to-propane ratio.

To investigate the unapparent classes (including chemical components and reaction conditions) in the dataset, unsupervised learning methods are introduced for detailed grouping and visualizing. A *k*-mean clustering algorithm was used first to separate the data into clusters. As shown in Fig. S3,† different cluster numbers between 1 and 20 were tried, and the score *versus* cluster numbers were collected. The lower the score value the better the prediction. Thus, it is evident that above 5 clusters, there is only slight improvement, and 5 clusters were chosen for further PCA and *t*-SNE analysis.

PCA and *t*-SNE were used to reduce the dimensionality of the dataset to two and allow a 2-dimensional representation for the whole dataset. As shown in Fig. 3, it is quite clear that these 270 data points can be separated well into five classes. Unfortunately, it is hard to transform the conclusion from 2-dimensional back to full-dimensional space. The original reaction conditions, as well as chemical composition, can be colored concerning the cluster number we found by *k*-means clustering (Fig. 4 and S4†). It can be seen that one cluster would be propane concentration with pure propane in use (cluster 3, Fig. 4b), and another cluster would be WHSV at high values (cluster 4, Fig. 4c). It is clear to see that the clustering is not heading for the classes containing just one factor but for multi-component catalyst classes. This makes the interpretation somehow difficult. Although some insight into the dataset can be gained with clustering, supervised algorithms are urgently needed to make predictions based on the whole dataset.

### 3.2 Supervised learning with different algorithms

Supervised learning algorithms are used for further prediction and analysis. The dataset was separated into the training set and testing set to verify the accuracy. Four different algorithms, including artificial neural network (ANN), support vector regressor (SVR), random forest regressor (RF) and *k*-nearest neighbor (KNN) were used to predict the STY values (Fig. 5). The root-mean-squared-error (RMSE) and *R*<sup>2</sup> score of all the

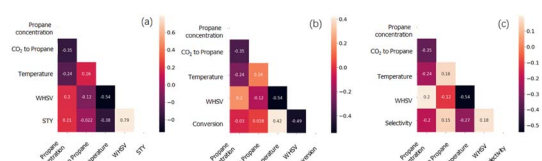


Fig. 2 Heatmap of Pearson correlation between reaction conditions and (a) STY value, (b) propane conversion, and (c) propylene selectivity. The colors present the correlation between two factors. Specifically, the deep intensity of the color represents their negative correlation, and the light intensity of the color represents their positive correlation.

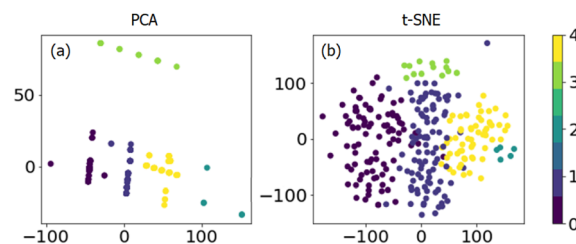


Fig. 3 Dimensional reduction of the dataset by (a) PCA and (b) *t*-SNE from *k*-means clustering (color bar); different colors indicate different classes.



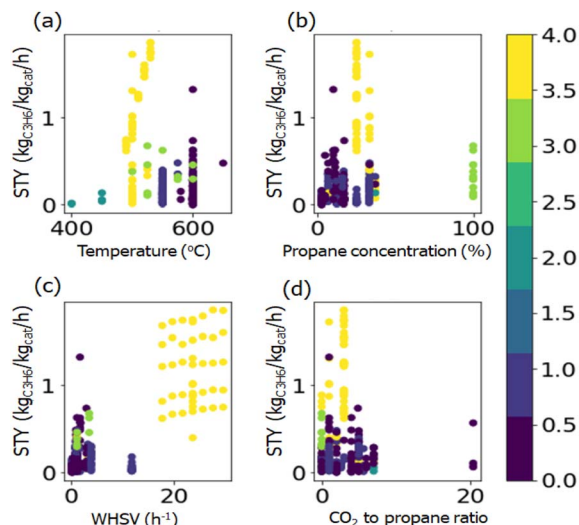


Fig. 4 Coloring the reaction conditions of (a) temperature, (b) propane concentration, (c) WHSV, and (d) CO<sub>2</sub> to propane ratio with respect to the cluster analysis. Different colors indicate different classes.

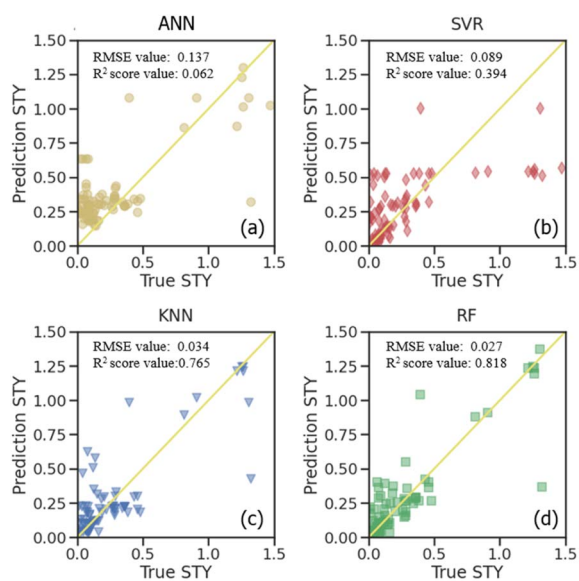


Fig. 5 Predictions with machine learning model of (a) ANN, (b) SVR, (c) KNN and (d) RF on the testing set.

algorithms were compared in both the training set and testing set shown in Fig. 6. Lower RMSE and higher  $R^2$  score indicate better prediction ability for the algorithm.

Fig. 5 illustrates a comparison of the prediction quality for different algorithms on the STY value in the testing set. The true STY values are plotted on the “x” axis, and the predicted ones on the “y” axis. It can be seen that all of them possess a decent prediction quality. Specifically, the RF algorithm seems to perform a better precision, while ANN and the SVR both exhibited deviations for the STY values. It is suggested that the STY values and corresponding deviations possess a monotonic increment under these predictions, which might be due to the

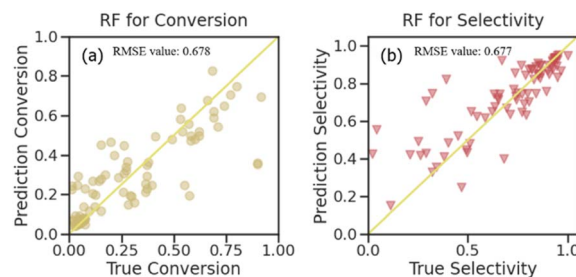


Fig. 6 Predictions for the RF algorithm used on the testing set (a) propane conversion and (b) propylene selectivity.

less frequent samples with very high STY values in the original data.

For further comparison, the STY prediction ability of the four machine learning models presenting as RMSE and  $R^2$  scores are shown in Fig. S5.† The results for the predicting training data and the testing data are presented. These values from the training dataset show how adequately the model is fitted to the data, and the ones for the testing dataset show how well the model can predict a new dataset. It is observed from the STY behavior that ANN has the highest RMSE values on both the training set and testing set (0.158 and 0.137, respectively). It also shows the worst  $R^2$  score values among all the algorithms with 0.199 and 0.062 on the training set and testing set, respectively. This indicates that ANN is the worst algorithm for STY prediction in CO<sub>2</sub>-ODHP. KNN showed the same prediction ability on both the training set and testing set with similar RMSE and  $R^2$  score values. For SVR, although it possesses a good ability in training sets with an RMSE of 0.005 and an  $R^2$  score of 0.975, the prediction ability for the new dataset, that is the testing set herein, is poor. Its RMSE is 0.089 with an  $R^2$  score of 0.394. The RF model performs best among the four models for the STY value prediction. It showed the lowest RMSE value and the highest  $R^2$  score value on both the training set and testing set. Especially on the testing set, the RMSE value was only 0.027 and the  $R^2$  score was 0.818, exhibiting good prediction ability for STY values in CO<sub>2</sub>-ODHP.

With the results of the STY value prediction, the RF algorithm was chosen for further investigation on propane conversion and propylene selectivity prediction. The comparative evaluation of the prediction capabilities of the RF algorithm on the testing dataset using the joint scatter plots of the actual values *versus* predicted ones is shown in Fig. 6. The plots revealed that the RF algorithm results in accurate predictions for propane conversion and propylene selectivity. Shown as the  $R^2$  score (Fig. S6†), the goodness of fit for the RF model on the training data of propane conversion and propylene selectivity were 0.958 and 0.954, respectively, and for the testing data, they were 0.678 and 0.677, respectively. With RMSE evaluation, the accuracy of the RF model on propane conversion and propylene selectivity were both lower than 0.025. These can further substantiate the fact that except for STY value, the RF model is also suitable for the prediction of propane conversion and propylene selectivity.



### 3.3 Interpretability of the RF model with SHAP

To understand the RF predictions in detail, we utilized the SHapley Additive exPlanations (SHAP) interpretation method to decompose the predicted value into the additive sum of the contributions from individual feature values. SHAP can provide global interpretability, and the dependence of the target output can be explained in terms of the features. The importance of the evaluated features was clarified by sorting them in descending order. It can also give visualization to the impact of the predicted STY values, propane conversion and propylene selectivity on the value of each descriptor (Fig. 7). The overall impact of each descriptor can be calculated by normalizing the Shapley values (abbreviated as SHAP values). A higher SHAP value of the descriptor means a more important influence on model prediction and *vice versa*.

Fig. 7a, c and e clearly show that CO<sub>2</sub>-ODHP is strongly controlled by the experimental conditions of WHSV and the reaction temperature. These two features are both located as the top 5 important features for STY, propane conversion and propylene selectivity, which might be due to the equilibrium of CO<sub>2</sub>-ODHP and side reactions. Moreover, the correlation between the features and their global impact based on the calculated SHAP values are also given in Fig. 7b, d and f.

For the STY value in Fig. 7a and b, it can be seen that with an increase of WHSV (blue dots to red dots), its contribution towards STY increases as indicated by the increase in SHAP values. That is, a high WHSV can result in a higher contribution towards STY compared to the average contribution as indicated by the positive SHAP values. In terms of the catalyst

composition, Cr, V, and Ce are found to be important in the STY dataset. Especially for Cr and V loading, a higher amount of these elements can improve the resulting STY.

Although WHSV is the most important feature for propane conversion (as shown in Fig. 7c and d), it has a negative impact, as most of the blue dots (lower WHSV) are located on the right side and red ones (higher WHSV) are on the left side. It should be noted that except for the reaction conditions, high Zn content and V content would lead to a higher SHAP value, indicating more Zn or V species can improve the conversion of propane, which may provide insight into CO<sub>2</sub>-ODHP.

Propylene selectivity is also an important indicator in CO<sub>2</sub>-ODHP, and the feature importance differs from STY and propane conversion, as shown in Fig. 7e and f. For the effect of the reaction conditions, high WHSV and high reaction temperature (red dots) are suggested to cause low SHAP value, indicating the negative impact of these reaction conditions on propylene selectivity. For the chemical components, Cr content is the most important feature among all the features in determining propylene selectivity due to its greatest average impact on the model output, as indicated by the mean absolute SHAP values. However, Ce, Zn and Ni show a negative impact. According to the above analysis, it can be inferred that the efficient exploration of high-performance catalytic systems is still challenging owing to the multiple effects of reaction conditions. Moreover, it is well known that machine learning is representative of the given data in the dataset, and it remains difficult to design novel catalysts far away from the input data. However, machine learning for catalyst component prediction can provide insight into the influence of the metal type and metal content, which thus gives a great chance for predicting the roles of new types of active components, and further investigation (such as Zn-based catalysts in CO<sub>2</sub>-ODHP) would be necessarily desirable.

## 4 Conclusions

In this study, we used four kinds of machine learning algorithms including artificial neural network (ANN), *k*-nearest neighbors (KNN), support vector regression (SVR) and random forest regression (RF) to predict the STY values with collected reported data of CO<sub>2</sub>-ODHP reaction. Notably, the RF model evaluated by RMSE and *R*<sup>2</sup> score was considered the preferred model for further investigation due to its superior performance compared with the other three models. The RF model also provided a good match for propane conversion and propylene selectivity prediction with its decent ability of prediction. For the model interpretation, a widely used SHAP algorithm based on the Shapley value on random forest regression prediction was introduced to rank the input features according to their impact on the output values. The reaction conditions, including WHSV, and reaction temperature were found to be important for catalytic performance, and identified as the top 5 features. For chemical components, Zn, V, Ni, *etc.* possess a positive impact, while the Ce content has a negative impact on different output variables, which can be fine-tuned in the future to prepare catalysts with high activity. The present work provides

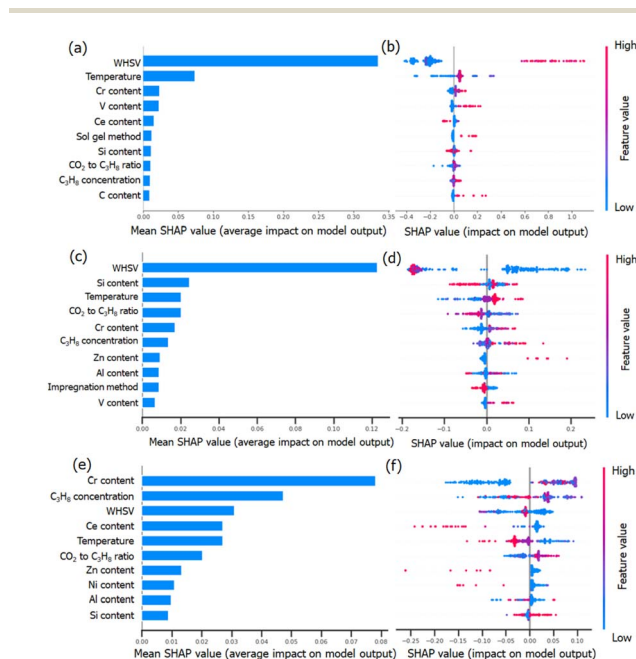


Fig. 7 Bar plot of the features based on their importance calculated with the mean absolute SHAP values for (a) STY value, (c) propane conversion and (e) propylene selectivity. A summary plot between feature value and their impact on the output value for (b) STY value, (d) propane conversion and (f) propylene selectivity (with the only top 10 features are displayed).



a great perspective for data analysis with machine learning in the CO<sub>2</sub>-ODHP reaction, and provides a reliable strategy for identifying the relationship of property-performance hidden in the vast data from the literature.

## Conflicts of interest

There are no conflicts to declare.

## Acknowledgements

This work is supported by the National Engineering Research Center for Petroleum Refining Technology and Catalyst (RIPP, SINOPEC) with no. 33600000-23-FW2313-0001, and the State Key Laboratory of Heavy Oil Processing, China University of Petroleum.

## Notes and references

- 1 T. Otroshchenko, G. Jiang, V. A. Kondratenko, U. Rodemerck and E. V. Kondratenko, *Chem. Soc. Rev.*, 2021, **50**, 473–527.
- 2 X. Jiang, L. Sharma, V. Fung, S. J. Park, C. W. Jones, B. G. Sumpter, J. Baltrusaitis and Z. L. Wu, *ACS Catal.*, 2021, **11**, 2182–2234.
- 3 C. Li and G. Wang, *Chem. Soc. Rev.*, 2021, **50**, 4359–4381.
- 4 J. Sheng, B. Yan, W.-D. Lu, B. Qiu, X.-Q. Gao, D. Wang and A.-H. Lu, *Chem. Soc. Rev.*, 2021, **50**, 1438–1468.
- 5 E. Gomez, B. H. Yan, S. Kattel and J. G. G. Chen, *Nat. Rev. Chem.*, 2019, **3**, 638–649.
- 6 M. A. Atanga, F. Rezaei, A. Jawad, M. Fitch and A. A. Rownaghi, *Appl. Catal., B*, 2018, **220**, 429–445.
- 7 J. Baek, H. J. Yun, D. Yun, Y. Choi and J. Yi, *ACS Catal.*, 2012, **2**, 1893–1903.
- 8 Q. Zhu, M. Takiguchi, T. Setoyama, T. Yokoi, J. N. Kondo and T. Tatsumi, *Catal. Lett.*, 2011, **141**, 670–677.
- 9 M. L. Balogun, S. Adamu, M. S. Ba-Shammakh and M. M. Hossain, *J. Ind. Eng. Chem.*, 2021, **96**, 82–97.
- 10 Z.-F. Han, X.-L. Xue, J.-M. Wu, W.-Z. Lang and Y.-J. Guo, *Chin. J. Catal.*, 2018, **39**, 1099–1109.
- 11 P. Michorczyk, P. Kuśtrowski, A. Kolak and M. Zimowska, *Catal. Commun.*, 2013, **35**, 95–100.
- 12 S. Orlyk, M. Kantserova, V. Chedryk, P. Kyriienko, D. Balakin, Y. Millot and S. Dzwigaj, *J. Porous Mater.*, 2021, **28**, 1511–1522.
- 13 M. Kantserova, N. Vlasenko, S. Orlyk, K. Veltruska and I. Matolinova, *Theor. Exp. Chem.*, 2019, **55**, 207–214.
- 14 M. Chen, J.-L. Wu, Y.-M. Liu, Y. Cao, L. Guo, H.-Y. He and K.-N. Fan, *Appl. Catal., A*, 2011, **407**, 20–28.
- 15 K. K. Bu, Y. K. Kang, Y. F. Li, Y. H. Zhang, Y. Tang, Z. Huang, W. Shen and H. L. Xu, *Appl. Catal., B*, 2024, **343**, 123528.
- 16 S. Lawson, K. Baamran, K. Newport, T. Alghamadi, G. Jacobs, F. Rezaei and A. A. Rownaghi, *Appl. Catal., B*, 2022, **303**, 120907.
- 17 M. M. Sullivan and A. Bhan, *J. Catal.*, 2018, **357**, 195–205.
- 18 H. Mai, T. C. Le, D. Chen, D. A. Winkler and R. A. Caruso, *Chem. Rev.*, 2022, **122**, 13478–13515.
- 19 J. A. Esterhuizen, B. R. Goldsmith and S. Linic, *Nat. Catal.*, 2022, **5**, 175–184.
- 20 Y. N. Guan, D. Chaffart, G. H. Liu, Z. Y. Tan, D. S. Zhang, Y. J. Wang, J. D. Li and L. Ricardez-Sandoval, *Chem. Eng. Sci.*, 2022, **248**, 117224.
- 21 Z. C. Yu and W. M. Huang, *Electroanalysis*, 2022, **34**, 599–607.
- 22 R. Palkovits and S. Palkovits, *ACS Catal.*, 2019, **9**, 8383–8387.
- 23 B. V. Ayodele, M. A. Alsaffar, S. I. Mustapa, R. Kanthasamy, S. Wongsakulphasatch and C. K. Cheng, *Chem. Eng. Process.*, 2021, **166**, 108484.
- 24 K. W. Ting, H. Kamakura, S. S. Poly, M. Takao, S. H. Siddiki, Z. Maeno, K. Matsushita, K.-i. Shimizu and T. Toyao, *ACS Catal.*, 2021, **11**, 5829–5838.
- 25 H. Li, Z. Zhang and Z. J. Liu, *Catalysts*, 2017, **7**, 306.
- 26 A. Chakkingal, P. Janssens, J. Poissonnier, M. Virginie, A. Y. Khodakov and J. W. Thybaut, *Chem. Eng. J.*, 2022, **446**, 137186.
- 27 Y. Guo, X. R. He, Y. M. Su, Y. H. Dai, M. C. Xie, S. L. Yang, J. W. Chen, K. Wang, D. Zhou and C. Wang, *J. Am. Chem. Soc.*, 2021, **143**, 5755–5762.
- 28 N. K. Pandit, D. Roy, S. C. Mandal and B. Pathak, *J. Phys. Chem. Lett.*, 2022, **13**, 7583–7593.
- 29 D. Wang, R. Cao, S. Hao, C. Liang, G. Chen, P. Chen, Y. Li and X. Zou, *Green Energy Environ.*, 2021, **8**(3), 820–830.
- 30 H. S. Feng, H. Ding, S. Wang, Y. J. Liang, Y. Deng, Y. S. Yang, M. Wei and X. Zhang, *ACS Appl. Mater. Interfaces*, 2022, **14**, 25288–25296.
- 31 D. X. Chen, P. L. Kang and Z. P. Liu, *ACS Catal.*, 2021, **11**, 8317–8326.
- 32 Q. Y. Liu, C. Shang and Z. P. Liu, *J. Am. Chem. Soc.*, 2021, **143**, 11109–11120.
- 33 Q. X. Yang, A. Skrypnik, A. Matvienko, H. Lund, M. Holena and E. V. Kondratenko, *Appl. Catal., B*, 2021, **282**, 119554.
- 34 C. Jiang, H. Song, G. Sun, X. Chang, S. Zhen, S. Wu, Z. J. Zhao and J. Gong, *Angew. Chem., Int. Ed.*, 2022, e202206758.
- 35 X. Jiang, Y. Wang, B. R. Jia, X. H. Qu and M. L. Qin, *ACS Appl. Mater. Interfaces*, 2022, **14**(36), 41141–41148.
- 36 F. Pedregosa, G. Varoquaux, A. Gramfort, V. Michel, B. Thirion, O. Grisel, M. Blondel, P. Prettenhofer, R. Weiss and V. Dubourg, *J. Mach. Learn. Res.*, 2011, **12**, 2825–2830.
- 37 D. Arthur and S. Vassilvitskii, *k-means++: The advantages of careful seeding*, *Soda*, 2007, vol. 7, pp. 1027–1035.
- 38 L. v. d. Maaten, *J. Mach. Learn. Res.*, 2008, **9**, 2579–2605.
- 39 S. M. Lundberg and S.-I. Lee, *Proceedings of the 31st International Conference on Neural Information Processing Systems*, 2017, pp. 4765–4774.
- 40 S. M. Lundberg, G. Erion, H. Chen, A. DeGrave, J. M. Prutkin, B. Nair, R. Katz, J. Himmelfarb, N. Bansal and S.-I. Lee, *Nat. Mach. Intell.*, 2020, **2**, 56–67.
- 41 V. Vapnik, *Statistical learning theory*, Wiley, New York, 1998, vol. 1(624), p. 2.
- 42 L. Breiman, *Mach. Learn.*, 2001, **45**, 5–32.
- 43 M. T. Dickerson, R. S. Drysdale and J.-R. Sack, *Int. J. Comput. Geom. Appl.*, 1992, **2**, 221–239.

